PARP1-dependent recruitment of KDM4D histone demethylase to DNA damage sites promotes double-strand break repair

Hanan Khoury-Haddad[a], Noga Guttmann-Raviv[a], Inbal Ipenberg[a], David Huggins[b], Anand D. Jeyasekharan[c,d], and Nabieh Ayoub[a,1]

[a]Department of Biology, Technion-Israel Institute of Technology, Haifa 32000, Israel; [b]Department of Oncology, Hutchison/Medical Research Council Research Centre, Cambridge CB2 0XZ, United Kingdom; [c]Department of Haematology-Oncology, National University Hospital, Singapore 119228; and [d]Cancer Science Institute, National University of Singapore, Singapore 119077

Edited by Richard D. Kolodner, Ludwig Institute for Cancer Research, La Jolla, CA, and approved January 14, 2014 (received for review September 19, 2013)

Members of the lysine (K)-specific demethylase 4 (KDM4) A–D family of histone demethylases are dysregulated in several types of cancer. Here, we reveal a previously unrecognized role of KDM4D in the DNA damage response (DDR). We show that the C-terminal region of KDM4D mediates its rapid recruitment to DNA damage sites. Interestingly, this recruitment is independent of the DDR sensor ataxia telangiectasia mutated (ATM), but dependent on poly (ADP-ribose) polymerase 1 (PARP1), which ADP ribosylates KDM4D after damage. We demonstrate that KDM4D is required for efficient phosphorylation of a subset of ATM substrates. We note that KDM4D depletion impairs the DNA damage-induced association of ATM with chromatin, explaining its effect on ATM substrate phosphorylation. Consistent with an upstream role in DDR, KDM4D knockdown disrupts the damage-induced recombinase Rad51 and tumor protein P53 binding protein foci formation. Consequently, the integrity of homology-directed repair and nonhomologous end joining of DNA breaks is impaired in KDM4D-deficient cells. Altogether, our findings implicate KDM4D in DDR, furthering the links between the cancer-relevant networks of epigenetic regulation and genome stability.

histone demethylation | chromosome instability | PARylation

Our genome is constantly attacked by intracellular and external mutagens; therefore, failure to sense and/or accurately repair DNA damage could lead to the accumulation of mutations and genetic instability that fuel tumorigenesis (1). Vertebrate cells use at least two distinct pathways for the repair of double-strand breaks (DSBs). The first is nonhomologous end joining (NHEJ), which is an error-prone process. The second is homology-directed repair (HDR), an error-free process that functions only in S and G2 phases of the cell cycle (2).

DNA damage induces rapid and highly orchestrated changes in chromatin structure that initiate the DNA damage response (DDR) and promotes the accumulation of various DNA repair proteins at sites of damage (3). Such chromatin changes are regulated by several mechanisms, including posttranslational modifications (PTMs) of histones and histone-binding proteins (4–6). For instance, lysine methylation of both histone and nonhistone proteins has been implicated in DDR (7–11). Histones are mono, di-, or trimethylated on their lysine residues, which generates binding sites for different histone-binding proteins, usually triggering either condensation or decondensation of chromatin. Differential methylation patterns of histones mark distinct regions and transcriptional states in the genome (12–14). Trimethylation of histone H3 on lysine 9 (H3K9me3) is enriched in condensed pericentric heterochromatin whereas di- and monomethylation of H3K9 (H3K9me2/1) are associated with transcriptionally silent domains within euchromatin (13, 15). An entirely new family of *Jmj*C domain-containing histone demethylases, which can demethylate di- and trimethylated lysines, has been recently discovered (16, 17). The lysine (K)-specific demethylase 4 (KDM4) family (KDM4A to -D; also known as JMJD2A to -D) members specifically demethylate H3K9me2/me3 and H3K36me2/me3 (16-21). KDM4A, -B, and -C encode proteins consisting of a JmjN, a JmjC, two PHD, and two Tudor domains whereas KDM4D encodes a shorter protein (523 aa) consisting only of JmjN and JmjC domains (16). The JmjC domain forms a pocket, which coordinates Fe^{2+} and α-ketoglutarate (α-KG), and catalyzes the removal of a methyl group from lysine by a hydroxylation reaction (17). Remarkably, members of the KDM4 family are up-regulated in different types of human cancer, and, importantly, their depletion impairs cancer-cell proliferation and tumor formation (18–20, 22–27). Moreover, several observations implicating histone demethylation in DDR have been recently reported (19, 28, 29). Of particular interest, it was recently shown that, in response to DNA damage, KDM4A and KDM4B undergo rapid degradation that facilitates foci formation of tumor protein P53 binding protein (53BP1) (30).

Here, we present a previously unrecognized role of KDM4D in HDR and NHEJ of DSBs. We show that KDM4D is rapidly recruited to sites of DNA damage independent of its demethylase activity. This recruitment is regulated by PARP1-mediated poly-ADP ribosylation (PARylation) of the C terminus of KDM4D. Moreover, we found that KDM4D knockdown sensitizes cells to DNA damage, inhibits the DNA damage-induced accumulation of ataxia telangiectasia mutated (ATM) at chromatin, and impairs the phosphorylation of ATM substrates H2AX, Krüppel associated box-associated protein 1 (KAP1), and checkpoint kinase 2 (Chk2).

Significance

Sophisticated DNA damage repair mechanisms are required to fix DNA lesions and preserve the integrity of the genome. This manuscript provides characterization of KDM4D role in promoting the repair of double-strand breaks (DSBs). Our findings show that KDM4D lysine demethylase is swiftly recruited to DNA breakage sites via its C-terminal region in a PARP1-dependent manner. Further, we have uncovered an exciting function of KDM4D in regulating the association of the DNA damage response master kinase, ATM, with chromatin, thus explaining the defective phosphorylation of ATM substrates found in KDM4D-depleted cells. Altogether, this study advances our understanding of the molecular mechanisms that regulate the repair of DSBs, a critical pathway that is essential for maintaining genome integrity.

Author contributions: H.K.-H., N.G.-R., and N.A. designed research; H.K.-H., N.G.-R., and I.I. performed research; D.H. performed structural analysis of the JmjC domain to generate demethylase-dead mutant; H.K.-H., N.G.-R., A.D.J., and N.A. analyzed data; and N.A. wrote the paper.

The authors declare no conflict of interest.

This article is a PNAS Direct Submission.

[1]To whom correspondence should be addressed. E-mail: ayoubn@tx.technion.ac.il.

This article contains supporting information online at www.pnas.org/lookup/suppl/doi:10.1073/pnas.1317585111/-/DCSupplemental.

Also, KDM4D depletion affects the timely formation of damage-induced foci of recombinase Rad51 and 53BP1 proteins and the integrity of HDR and NHEJ of DSBs in cells. Altogether, this study advances our understanding of the molecular mechanisms that regulate DSB repair, a critical pathway that is essential for maintaining genome integrity.

Results

EGFP-KDM4D Is Rapidly Recruited to Laser-Microirradiated Regions. We sought to determine whether DNA damage influences the cellular localization of KDM4D protein. Toward this end, we established a stable U2OS-TetON cell line that conditionally expresses functional EGFP-KDM4D fusion (Tables S1 and S2). Western blot and immunofluorescence (IF) analyses reveal that EGFP-KDM4D expression is induced only upon the addition of doxycycline and causes a significant decrease in the levels of H3K9me3 mark (Fig. S1). We then set up a laser-microirradiation assay to induce targeted DNA damage as evident by the formation of the phosphorylated form of histone H2AX (γH2AX) and the recruitment of MDC1 repair protein (Fig. S2 *A* and *B*).

Time-lapse imaging shows that laser microirradiation leads to a rapid accumulation (within 15 s) of EGFP-KDM4D at sites of DNA damage. This result demonstrates that EGFP-KDM4D recruitment is an early event in the DNA damage-signaling cascade (Fig. 1*A*). Similarly, recruitment of KDM4D to laser-irradiated regions was also observed in WI-38 cells (normal human diploid cells) and immortalized mouse embryonic fibroblasts (MEFs), transiently expressing EGFP-KDM4D (Fig. 1 *B* and *C*). Quantitative measurements of the fluorescence intensity at DNA damage sites reveal that EGFP-KDM4D is rapidly accumulated, reaching maximum levels around 60 s after laser microirradiation, except in WI-38 cells, which show slightly slower accumulation kinetics (Fig. 1 *A*–*C*, *Right*). The fold increase in the intensity of EGFP-KDM4D at laser-microirradiated sites is comparable with that of EGFP-MDC1 (Fig. S2*B*) and to other known DDR proteins (31, 32). Interestingly, EGFP-KDM4D accumulation at laser-microirradiated sites is transient. Time-lapse images show dispersal of KDM4D from DNA breakage sites within 30 min after damage induction (Fig. S2*C*). U2OS-TetON cells expressing nuclear EGFP (EGFP fused to a nuclear localization signal) were used as a control and show no discernible changes in the abundance of EGFP at laser-microirradiated regions (Fig. S2*D*). Altogether, these results provide a firm evidence that the rapid accumulation of KDM4D at sites of DNA damage is a widespread biological event, and not specific to a particular cell line. In addition, our results show that the recruitment of KDM4D to sites of damage is conserved between human and mouse cells.

Next, we wanted to assess whether, similar to EGFP-KDM4D fusion, the endogenous KDM4D protein is recruited to laser-microirradiated sites. To do so, we first confirmed the specificity and the suitability of KDM4D antibody (Ab-93694; Abcam) for Western blot and IF analyses (Fig. S3, Table S3, and *SI Materials and Methods*). U2OS and A172 cells (human glioblastoma cell lines that show high expression level of KDM4D protein) were seeded on a dish with a gridded coverslip, subjected to laser microirradiation, fixed, and costained for γH2AX and KDM4D. Results demonstrate that laser-irradiated regions, which are positive for γH2AX, show accumulation of the endogenous KDM4D protein in both U2OS and A172 cell lines (Fig. 1*D*). In agreement with these findings, chromatin fractionation shows that the amount of KDM4D protein in the chromatin-bound fraction increases after exposing cells to etoposide, which primarily generates DSBs (Fig. 1*E*). Importantly, the accumulation of KDM4D at the chromatin fraction is not due to an increase in overall protein levels of KDM4D after etoposide treatment (Fig. S3*E*). Similarly, the overall levels of KDM4D remain constant after DNA damage inflicted by ionizing radiation (IR) (Fig. S3*F*). Therefore, we

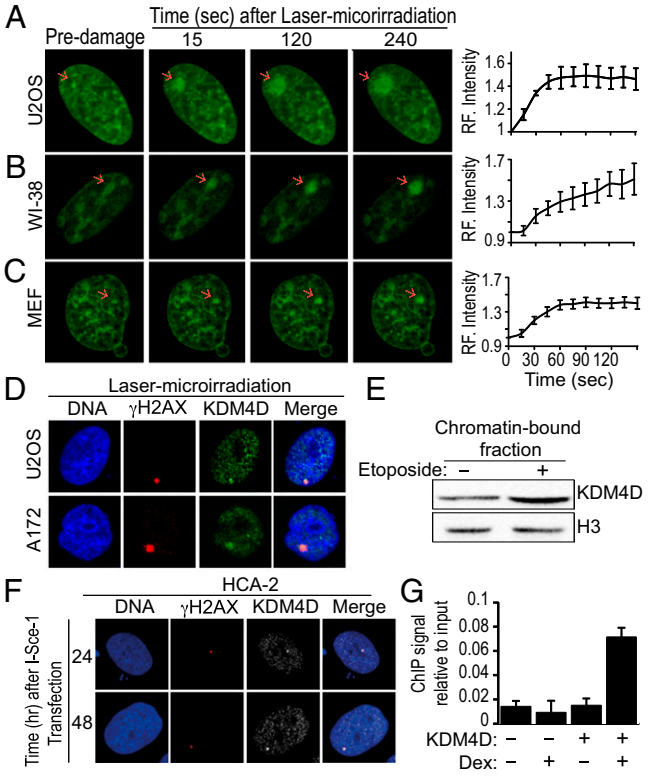

Fig. 1. KDM4D Protein is rapidly recruited to sites of DNA damage. (*A*–*C*) Time-lapse images show the localization of EGFP-KDM4D fusion at the indicated time points after the induction of laser DNA damage to a single region, marked by a red arrow. Graphs (*Right*) show fold increase in the relative fluorescence intensity of EGFP-KDM4D at laser-microirradiated sites. Each measurement is representative of at least 10 cells. Error bars indicate SD. (*A*) U2OS-TetON cells expressing EGFP-KDM4D fusion following the addition of doxycycline. Movie S1 shows the accumulation of full-length EGFP-KDM4D at the laser-microirradiated site. (*B* and *C*) WI-38 cells and MEFs transfected with expression vector encoding EGFP-KDM4D fusion. Results shown in *A*–*C* are typical of three independent experiments and represent at least 15 different cells each. (*D*) Recruitment of the endogenous KDM4D to laser-microirradiation sites. U2OS cells (*Upper*) and A172 cells (*Lower*) were fixed within 5 min after laser microirradiation and subjected to immunofluorescence analysis using antibodies against γH2AX (red) and KDM4D (green). (*E*) DNA damage-dependent increase in the levels of KDM4D protein in the chromatin-bound fraction. U2OS cells were exposed to 40 μM etoposide for 40 min and subjected to cellular fractionation as described in *Materials and Methods*. Chromatin-bound fractions from undamaged and DNA damaged cells were immunoblotted with KDM4D antibody. H3 is used as a loading control. (*F*) Representative pictures showing the recruitment of the endogenous KDM4D to a single DSB. A plasmid encoding for I-Sce-I endonuclease was transfected into HCA-2 fibroblast cells that contained a single recognition site for I-Sce-I endonuclease. Cells were fixed at 24 h (*Upper*) and 48 h (*Lower*) posttransfection and immunostained with γH2AX (red) and KDM4D (gray) antibodies. Results shown are typical of three independent experiments and represent at least 15 different cells. (*G*) ChIP analysis shows the binding of 6xmyc-KDM4D at DNA near DSBs induced by I-Sec-I endonuclease. U2OS-HR-ind cells were transfected with an expression vector encoding 6xmyc-KDM4D or with an empty vector that served as a negative control. Bars show the enrichment of KDM4D around the I-Sce-I recognition site. The cells were then treated for 30 min with Dex to allow the migration of I-Sce-I to the nucleus and the generation of DSBs at its recognition site. Cell lysates were then prepared and subjected to anti-myc ChIP followed by real-time PCR with primers adjacent to the I-Sce-I recognition site. The occupancy of 6xmyc-KDM4D adjacent to I-SceI–induced DSB was determined by quantitative real-time PCR analysis and normalized to GAPDH input DNA. Error bars represent SD from two independent experiments. Dex, dexamethasone; RF, relative fluorescence.

concluded that KDM4D accumulation at sites of DNA damage is not associated with an increase in its cellular levels.

Endogenous KDM4D Accumulates at a Single Double-Strand Break Site. To extend our observations, we sought to determine whether KDM4D is recruited to a single DSB. To do so, we took advantage of the immortalized human HCA-2 cell line, in which a single recognition site for I-Sce-I endonuclease is integrated (33). To induce a defined DNA break, HCA-2 cells were transfected with an expression vector encoding I-Sce-I endonuclease and stained for γH2AX and KDM4D. We observed that 64% and 80% of the cells (n = 50) that show a single γH2AX focus show also a colocalized accumulation of the endogenous KDM4D at 24 and 48 h after transfection, respectively (Fig. 1*F*). One reason that not all γH2AX foci also show accumulation of KDM4D could result from a different kinetics in the formation and dissolution of γH2AX and KDM4D at sites of DNA damage.

To further validate the recruitment of KDM4D to DSB sites, we performed KDM4D chromatin immunoprecipitation assay (ChIP), followed by quantitative real-time PCR using primers adjacent to the I-Sce-I recognition site. Because ChIP-grade KDM4D antibody is not available, we monitored the recruitment of KDM4D fused to six copies of myc epitope (6xmyc) in U2OS-HR-ind cells. One distinctive feature of U2OS-HR-ind cells is that they constitutively express a recombinant I-Sce-I endonuclease fused to the ligand-binding domain of the glucocorticoid receptor to ensure its cytoplasmic localization. Therefore, addition of dexamethasone (Dex) induces rapid migration of the recombinant I-Sce-I nuclease into the nucleus and rapid induction of DSB at its recognition site within the GFP expression cassette (34). Mock and Dex-treated U2OS-HR-ind cells expressing either empty vector or vector encoding 6xmyc-KDM4D were subjected to ChIP using myc antibody. Results show that addition of Dex to U2OS-HR-ind cells expressing 6xmyc-KDM4D leads to ~4.8-fold induction in the abundance of the sequences surrounding the I-Sce-I sites compared with Dex-untreated cells and after normalization with GAPDH. Such increase is absent in cells transfected with an empty vector (Fig. 1*G*). Altogether, our data show that the endogenous KDM4D is recruited to a single DSB and that this recruitment is not specific to the laser-microirradiation type of DNA damage.

The Demethylase Activity of KDM4D Is Dispensable for Its Recruitment to Sites of DNA Damage. We sought to determine whether KDM4D demethylase activity is involved in its recruitment to DNA breakage sites. Toward this end, we generated a KDM4D "demethylase-dead" mutant. Computational modeling of the crystal structure of the *JmjC* domain from KDM4A (PDB ID code, 2P5B) predicts that the Ser196Met mutation is expected to abolish an existing hydrogen-bond network, disrupting the coordination of α-KG within the catalytic site and consequently abrogating the demethylase activity. Given the strong conservation of the Jmj*C* domain among the KDM4 members, we anticipated that mutating the corresponding serine residue in KDM4D, Ser200, to methionine would generate a demethylase-dead mutant (Fig. S4*A*). Indeed, Western blot and IF analysis reveal that overexpression of the KDM4D-S200M mutant in U2OS cells has no detectable effect on H3K9me3 levels whereas overexpression of wild-type KDM4D leads to a dramatic decrease in the levels of H3K9me3 mark (Fig. S4 *B* and *C*). Next, we microirradiated U2OS cells expressing EGFP-KDM4D-S200M mutant and found that it is rapidly recruited to sites of DNA damage (Fig. 2*A*). Quantitative measurements show that the accumulation kinetics and the fold increase in the relative fluorescence intensity of EGFP-KDM4D-S200M fusion (Fig. 2*A*, *Right*) are comparable with the wild-type EGFP-KDM4D (Fig. 1*A*, *Right*). Moreover, we found that KDM4D-S200M accumulation at laser-microirradiated sites is transient as it disperses from DNA breakage sites within 30 min after damage induction. We therefore concluded that the demethylase activity of KDM4D is dispensable for both accumulation and dispersal from sites of DNA damage.

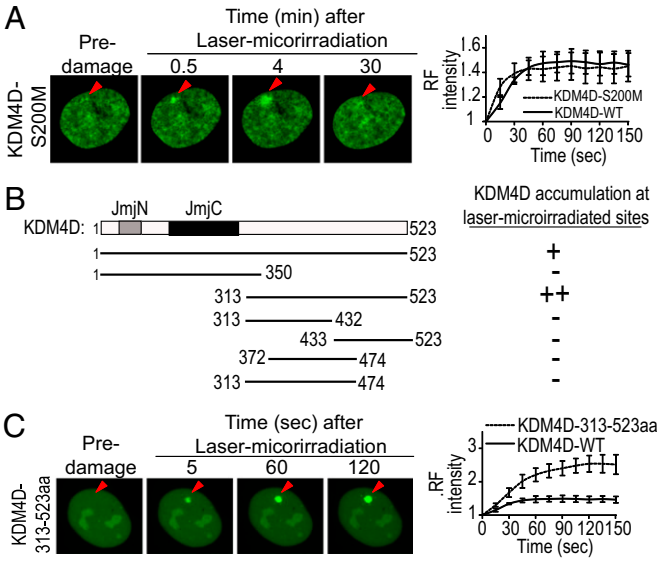

Fig. 2. The C-terminal, but not the demethylase activity, of KDM4D is essential and sufficient for its recruitment to DNA breakage sites. (*A*) A representative picture showing transient recruitment of the demethylase-dead mutant, KDM4D-S200M, to laser-microirradiated regions (marked with red arrowhead). Shown are time-lapse images of U2OS cells transfected with EGFP-KDM4D-S200M and subjected to laser-microirradiation. The graph shows the increase in the relative fluorescence intensity of EGFP-KDM4D-WT and EGFP-KDM4D-S200M at laser-microirradiated sites. Error bars represent SD of 10 different cells. (*B*) Deletion-mapping analysis showing that the C-terminal region of KDM4D is essential and sufficient for KDM4D recruitment to sites of DNA damage. U2OS cells were transfected with expression vector encoding EGFP fused to full-length or to the indicated fragments of KDM4D. Laser microirradiation was then applied, and the ability of the deletion mutants to accumulate at DNA breakage sites was assessed. (*C*) A representative picture showing the rapid recruitment of the C-terminal region of KDM4D (KDM4D$^{313\text{-}523}$) to laser-microirradiated regions. Results shown are typical of at least five independent experiments and represent more than 50 different cells. The graph shows the increase in the relative fluorescence intensity of EGFP-KDM4D-WT and EGFP- KDM4D$^{313\text{-}523}$ at laser-microirradiated sites. Error bars represent SD of 10 different cells for each fusion. Movie S2 shows the accumulation of EGFP-KDM4D$^{313\text{-}523}$ at the laser-microirradiated site. RF, relative fluorescence.

The C-Terminal Region of KDM4D Is Essential and Sufficient for Its Accumulation at Sites of DNA Damage. We performed deletion-mapping analysis to identify the region of KDM4D that regulates its recruitment to sites of DNA damage. Deletion mutants of KDM4D were tagged with EGFP and tested for recruitment to laser-microirradiated sites of DNA (Fig. 2*B*). Results show that the N-terminal and the middle region of KDM4D are unable to accumulate at laser-microirradiated sites. In contrast, we found that the C-terminal region encoding residues 313–523 aa of the KDM4D is essential and sufficient for its recruitment to DNA-damage sites (Fig. 2 *B* and *C*). Interestingly, EGFP-KDM4D$^{313\text{-}523aa}$ shows much faster and stronger accumulation at laser-microirradiated sites than the full-length EGFP-KDM4D fusion. EGFP-KDM4D$^{313\text{-}523aa}$ accumulation at damaged sites can be clearly visualized within 5 s after laser microirradiation (Fig. 2*C*, *Right*). Further deletions of the C-terminal region into smaller overlapping fragments abrogates the ability to undergo recruitment to sites of DNA damage (Fig. 2*B*). These results imply either that several motifs across the KDM4D$^{313\text{-}523aa}$ region are required for recruiting KDM4D to DNA breakage sites or that the integrity of the

domain is important and further deletions of the domain disturb its secondary structure.

ATM Kinase Is Not Essential for KDM4D Recruitment to DNA Damage Sites. Phosphatidylinositol 3-kinase–related kinases (PIKKs), such as ATM and ATR, regulate both the activity and recruitment of various DDR proteins to DNA damage sites (4). We sought therefore to assess whether ATM or ATR regulates KDM4D recruitment. To do so, cells were pretreated with caffeine, which blocks the activation of ATM/ATR, before laser microirradiation. Results show no detectable effect on the recruitment of KDM4D to laser-microirradiated sites (Fig. S5*A*). Next, we chemically inhibited ATM kinase activity using a highly specific inhibitor, KU-55933. As expected, KU-55933–treated cells show defective induction of ATM and H2AX phosphorylation after damage, compared with untreated cells (Fig. S5*B*). Similar to caffeine-treated cells, KDM4D recruitment is not impaired by ATM inhibition (Fig. S5*C*). Collectively, we concluded that PIKK family members ATM and ATR are not critical for the recruitment of KDM4D to sites of DNA damage.

PARP1 Activity Controls the Recruitment of KDM4D to Sites of DNA Damage. To determine whether PARP1, another key DDR protein (35), is involved in regulating the recruitment of KDM4D to DNA breakage sites, we devised two different approaches. First, we monitored the accumulation of KDM4D at DNA damage sites in PARP1-depleted cells. To deplete PARP1, U2OS-TetON-EGFP-KDM4D cells were transfected with PARP1 siRNA (Ambion), and maximal depletion of PARP1 protein was observed at 72 h after transfection (Fig. S5*D*). PARP1-depleted cells ($n = 50$) were subjected to laser microirradiation. As shown in Fig. 3*A*, PARP1 depletion leads to a striking decrease in the number of cells that show KDM4D accumulation at DNA damage sites, comparing to mock transfected cells. Second, we chemically inhibited PARP1/2 using Ku-0059436 inhibitor (PARPi). Results show that pretreating cells with PARPi was sufficient to severely abrogate the recruitment of both the full-length and the C-terminal region of KDM4D to sites of damage (Fig. 3 *B* and *C*). Similarly, PARPi treatment inhibits the recruitment of the endogenous KDM4D to DSBs induced by I-Sce-I endonuclease activity (Fig. 3*D*). These results altogether confirm that PARP1 activity is critical for KDM4D recruitment to DNA damage sites.

PARP1 ADP Ribosylates KDM4D in a DNA Damage-Dependent Manner. How does PARP1 mediate the recruitment of KDM4D to sites of DNA damage? Based on the aforementioned results (Fig. 3), we hypothesized that PARP1 ADP ribosylates (PARylates) KDM4D in response to DNA damage. To explore this hypothesis, we set up an in vitro PARylation assay and showed that 6xHis-KDM4D fusion undergoes PARylation in the presence of PARP1 and NAD^+ that serves as a donor of the ADP-ribose moiety (Fig. 4*A*). Next, we tested the ability of different parts of KDM4D to undergo PARylation. The first 350 aa fused to 6xHis tag (6xHis-$KDM4D^{1\text{-}350aa}$) show a low level of PARylation, which can be detected only following long exposure time (Fig. 4*B*). This result is consistent with a recent paper showing PARylation of the N-terminal region of KDM4D (36). On the other hand, the C-terminal region fused to GST (GST-$KDM4D^{348\text{-}523aa}$) undergoes massive PARylation whereas the GST is not PARylated (expressing the C-terminal of KDM4D fused to 6xHis tag proved unsuccessful), suggesting that KDM4D is primarily PARylated at its C-terminal region, in vitro (Fig. 4*C*).

On this basis, we hypothesize that KDM4D undergoes in vivo PARylation in response to DNA damage. To assess this hypothesis, U2OS-TetON cells expressing either EGFP-KDM4D or EGFP only were pretreated with either etoposide or camptothecin (CPT), which generates mainly single-strand breaks. Next, EGFP and EGFP-KDM4D fusion were purified using GFP-TRAP beads, and the immunoprecipitates were immunoblotted with PAR and GFP antibodies. Results show that DNA damage, triggered by either etoposide or CPT, induces PARylation of EGFP-KDM4D fusion whereas untreated cells show a basal level of EGFP-KDM4D PARylation (Fig. 4*D*). To further validate the in vivo PARylation of KDM4D, U2OS-TetON-EGFP-KDM4D cells were incubated with PARPi for 3 h before etoposide treatment. Results show that the DNA damage-induced PARylation of EGFP-KDM4D is severely suppressed in PARP-inhibited cells

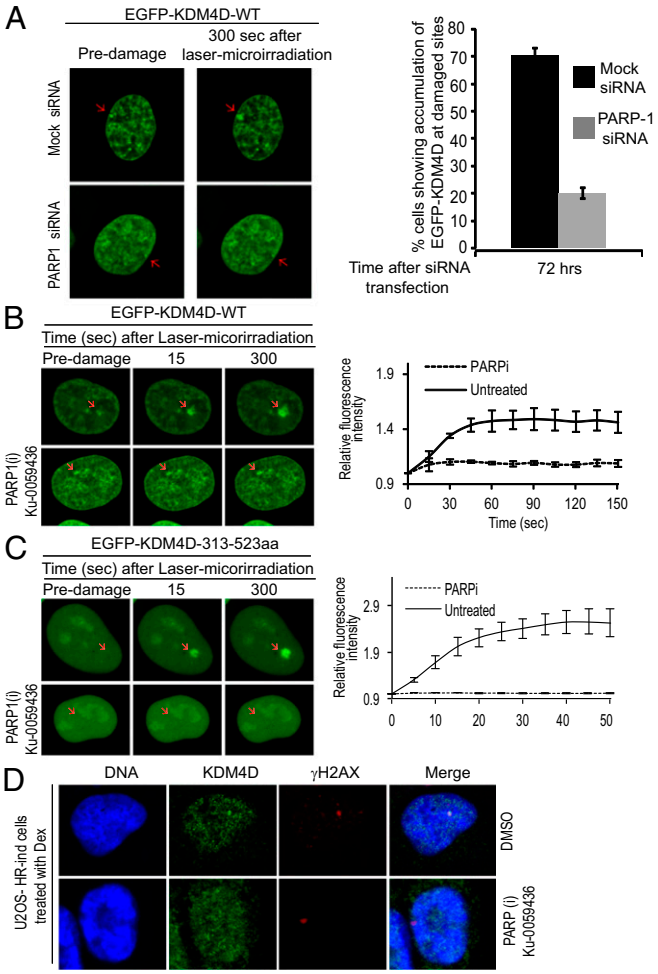

Fig. 3. PARP1-dependent recruitment of KDM4D to laser-microirradiated sites. (*A*) The effect of PARP1 siRNA knockdown on the recruitment of KDM4D to DNA damage sites. Representative time-lapse images show the recruitment of EGFP-KDM4D after laser microirradiation of mock and PARP1-depleted cells (marked by red arrow) (*Left*). The intensity of EGFP-KDM4D signal at the damaged area was measured using Carl Zeiss Zen software. The graph displays the percentage of PARP1-depleted cells that show accumulation of EGFP-KDM4D to laser-microirradiated regions, compared with mock transfected cells at 72 h after transfection (*Right*). Error bars represent the SEM from two independent experiments. (*B* and *C*) Chemical inhibition of PARP1/2 suppresses the recruitment of EGFP-KDM4D (*B*) and EGFP-$KDM4D^{313\text{-}523}$ (*C*) fusions to laser-microirradiated sites. U2OS-TetON cells expressing EGFP-KDM4D or EGFP-$KDM4D^{313\text{-}523}$ fusions were treated for 1 h with 5 μM PARP1/2 inhibitor, Ku-0059436. Representative time-lapse images show the localization of fusion proteins at the indicated times after laser microirradiation of a single region (marked by arrow). Results shown are typical of three independent experiments and represent at least 30 different cells. Graphs (*Right*) show fold increase in the relative fluorescence intensity of EGFP-KDM4D at laser-microirradiated sites. (*D*) PARP-dependent recruitment of the endogenous KDM4D to single-DSBs induced by I-Sce-I endonuclease, as described in Fig. 1*F*. Mock and PARPi-treated HR-ind cells were immunostained with γH2AX (red) and KDM4D (gray) antibodies. Results shown represent 15 different cells.

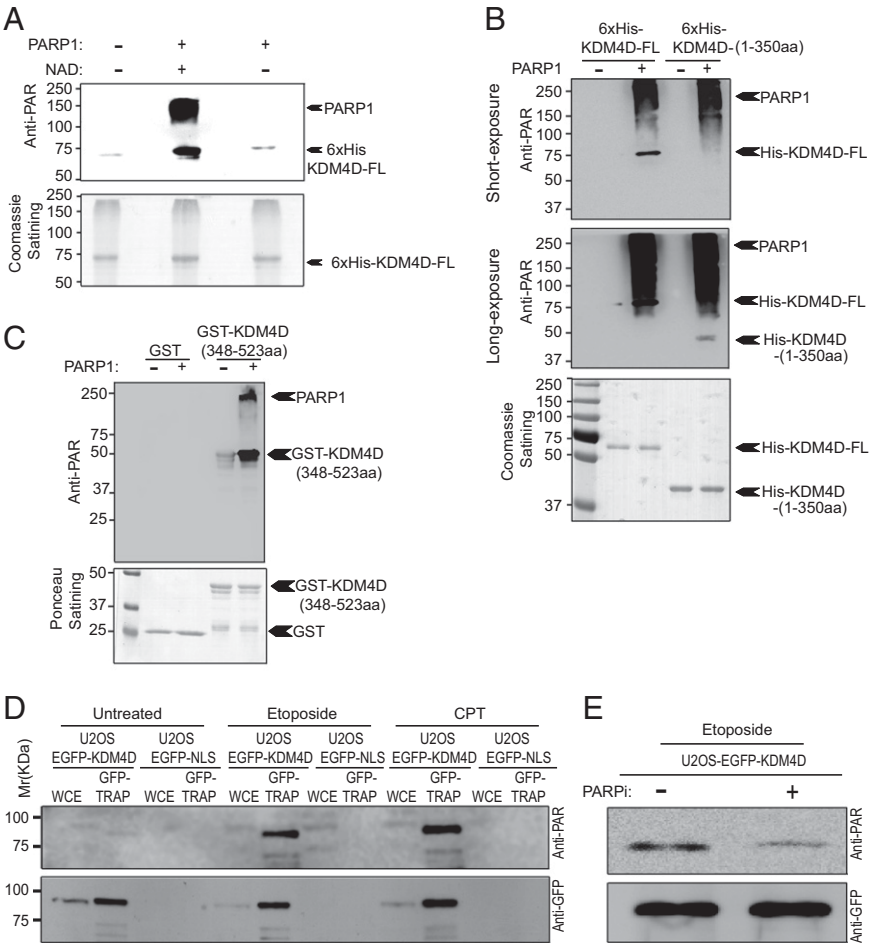

Fig. 4. KDM4D is PARylated in response to DNA damage. (*A–C*) In vitro PARylation of KDM4D using recombinant PARP1 enzyme in the presence or absence of either PARP1 or NAD^+. The reaction mixtures were immunoblotted using PAR antibody and stained with Coomassie (*A* and *B*) or Ponceau S (*C*) for loading control. (*A*) The full-length 6xHis-tagged KDM4D is PARylated in vitro. (*B*) In vitro PARylation of 6xHis-tagged $KDM4D^{1\text{-}350aa}$ protein only following long exposure time. (*C*) PARylation of the GST-tagged $KDM4D^{348\text{-}523aa}$ protein. GST tag was used as a negative control. (*D*) DNA damage-dependent PARylation of EGFP-KDM4D in cells. U2OS-TetON-EGFP-NLS and U2OS-TetON-EGFP-KDM4D cell lines were treated with etoposide or CPT genotoxic agents, subjected to GFP-TARP pull down, and immunoblotted using PAR antibody (*Upper*). Next, the membrane was stripped and immunostained with GFP antibody (*Lower*). (*E*) PARP inhibition suppresses the DNA damage-dependent PARylation of EGFP-KDM4D in cells. As in *D*, except that the cells were grown in the presence of 20 μM PARPi for 3 h before etoposide treatment.

(Fig. 4*E*). Altogether, these observations demonstrate that EGFP-KDM4D undergoes in vivo PARylation in response to DNA damage, a modification that might regulate KDM4D recruitment to DNA breakage sites.

PARylation of KDM4D Is Essential for Its Recruitment to Sites of DNA Damage. We sought to map KDM4D PARylation sites and to assess their effect on the accumulation of KDM4D at DNA damage regions. Given that KDM4D PARylation occurs mainly at its C terminus (Fig. 4*C*), we restricted our search for PARylated residues within this region. We performed multiple sequence alignments of the C-terminal region of KDM4D from several species and revealed seven evolutionary conserved residues (E357, R450, R451, R455, E464, K472, and R473) that can potentially undergo PARylation (Fig. S6*A*). Next, we substituted each of the conserved residues with alanine and tested their effect on the recruitment of $EGFP\text{-}KDM4D^{313\text{-}523aa}$ to laser-microirradiated sites. The $EGFP\text{-}KDM4D^{313\text{-}523aa}$ mutants K472A-R473A, R455A, or E357A show inefficient recruitment to sites of damage as evident by a significant reduction in the fluorescence intensity at the site of damage, compared with the wild-type (Fig. S6*D*). Interestingly, $EGFP\text{-}KDM4D^{313\text{-}523aa}$ mutant, including the four mutations R450A, R451A, E357A, and R455A (hereafter called KDM4D-4M), fails to accumulate at laser-microirradiated sites (Fig. 5*A*). Similarly, full-length EGFP-KDM4D-4M mutant lost its ability to accumulate at laser-microirradiated region (Fig. 5*B*). On the other hand, E464A mutation has no detectable effect on the recruitment of $EGFP\text{-}KDM4D^{313\text{-}523aa}$ to sites of DNA damage (Fig. S6*D*). Collectively, our analysis shows that R450A, R451A, E357A, and R455A residues are critical for $EGFP\text{-}KDM4D^{313\text{-}523aa}$ and the full-length EGFP-KDM4D recruitment whereas K472, R473, and E464 show a milder disruption of the recruitment of $EGFP\text{-}KDM4D^{313\text{-}523aa}$ to sites of DNA damage.

Driven by these observations, we hypothesize that KDM4D-4M mutant failed to accumulate at DNA breakage sites because they are unable to undergo PARylation. To test this hypothesis, full-length KDM4D-4M fused to 6xHis tag was subjected to in vitro PARylation assay. Western blotting analysis shows that KDM4D-4M mutant lost its ability to undergo PARylation compared with the wild-type KDM4D protein (Fig. 5*C*). These observations altogether provide strong evidence that E357, R450, R451, and R455 residues are required for KDM4D PARylation and recruitment to sites of DNA damage.

Next, we sought to address whether the demethylase activity of KDM4D-4M mutant, which is defective in recruitment to DNA damage sites, was affected. Toward this end, we set up an in vitro demethylation assay where the recombinant His-KDM4D-WT and His-KDM4D-4M protein were incubated with bulk histones and the efficiency of the demethylase activity was assessed by measuring the level of H3K9me3 using specific antibody. Results clearly show that the demethylase activity of KDM4D-4M is indistinguishable from that of the wild-type KDM4D protein (Fig. S6*B*). Moreover, transfecting U2OS cells with a construct expressing KDM4D-4M fused to DsRed-Monomer (MR-KDM4D-4M) revealed that the nuclear localization and the in vivo demethylase activity of KDM4D-4M remain intact (Fig. S6*C*). These results argue against improper folding of KDM4D-4M mutant. Collectively, we genetically uncoupled the two functional domains of KDM4D: the first includes the *JmjC* domain that catalyzes

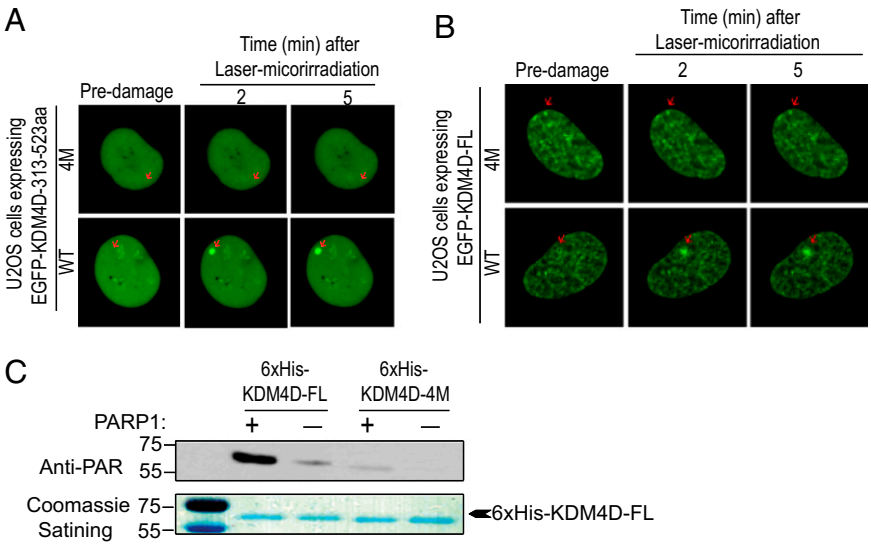

Fig. 5. KDM4D PARylation is essential for its recruitment to sites of DNA damage. (*A* and *B*) Alanine substitution of R450, R451, R455, and E357 (KDM4D-4M) abrogates the recruitment of EGFP-KDM4D$^{313\text{-}523aa}$ and full-length EGFP-KDM4D to laser-microirradiated sites. U2OS cells were transfected with expression vectors encoding either EGFP-KDM4D$^{313\text{-}523aa}$-4M (*A*, *Upper*), EGFP-KDM4D$^{313\text{-}523aa}$-WT (*A*, *Lower*), full-length EGFP-KDM4D-4M (*B*, *Upper*), or full-length EGFP-KDM4D-WT (*B*, *Lower*) and subjected to laser microirradiation (red arrow). Results shown are typical of three independent experiments and represent at least 30 different cells. (*C*) In vitro PARylation shows that PARylation of KDM4D-4M lost its ability to undergo PARylation, compared with the wild-type KDM4D protein. The reaction mixtures were either immunoblotted using PAR antibody (*Upper*) or stained with Coomassie (*Lower*).

the demethylation reaction and the second domain undergoes PARylation in response to DNA damage and targets KDM4D to DNA damage sites.

KDM4D Depletion Sensitizes Cells to Ionizing Radiation. A fundamental feature of any protein that functions in DDR is that its presence is required for cellular resistance to exogenous DNA damage. Thus, we sought to determine the effect of KDM4D depletion on cellular sensitivity to IR. Control and KDM4D-depleted cells (Fig. 6*A*) were subjected to increasing doses of IR, and cell survival was assessed using a clonogenic assay. We made two interesting observations. The first was that, irrespective of DNA damage, the viability of KDM4D-depleted cells was reduced by ∼55% compared with cells transfected with control siRNA (308 ± 47 colonies per dish compared with control cells at 141 ± 15 colonies per dish). The second observation was that, in response to IR, the ability of KDM4D-depleted cells to form colonies was significantly decreased compared with cells transfected with control siRNA (Fig. 6*B*). These results suggest that KDM4D-depleted cells are pronouncedly more sensitive to DNA damage induced by IR.

KDM4D Depletion Impairs the DNA Damage-Induced Phosphorylation of a Subset of ATM Substrates. To gain molecular insights into the mechanism by which KDM4D affects cellular sensitivity to DNA damage, we looked at the phosphorylation kinetics of early DNA damage markers. First, we assessed the autophosphorylation of ATM kinase on Ser-1981, which is known to be essential for intact DNA damage response (37). Results show that the levels of ATM-Ser1981 phosphorylation in KDM4D-depleted cells were indistinguishable from control cells. In contrast, we found that the phosphorylation levels of three well-characterized ATM substrates, H2AX-Ser139, KAP1-Ser824, and Chk2-Thr68, were profoundly reduced in KDM4D-depleted cells compared with control cells (Fig. 6 *D* and *E*). It should be noted that this reduction in the phosphorylation levels of ATM substrates is not due to a decrease in the total amount of ATM or its substrates (Fig. 6 *C*–*E*). Moreover, our results suggest that KDM4D depletion does not inhibit the kinase activity of ATM (Fig. 6*C*), but it inhibits the phosphorylation of a subset of ATM substrates. Altogether, these results are in agreement with the rapid recruitment of KDM4D to DNA breakage sites and suggest that KDM4D is involved in the initiation of the DNA damage-signaling cascade by facilitating the phosphorylation of the early markers of DNA damage.

KDM4D Promotes ATM Association with Chromatin. How does KDM4D affect ATM substrate phosphorylation? It has been reported that the levels of ATM protein at the chromatin-bound fraction increase in response to DNA damage (38). On this basis, we sought to address whether KDM4D affects the association of ATM with chromatin. To do so, control and KDM4D siRNA-treated U2OS cells were exposed to IR and subjected to biochemical fractionation followed by Western blot. Interestingly, KDM4D depletion leads to a severe reduction in the levels of ATM at the chromatin-bound fraction regardless of DNA damage. Also, KDM4D depletion inhibits the DNA damage-induced accumulation of ATM at chromatin. On the other hand, U2OS cells transfected with control siRNA show significant increase in the levels of ATM protein at the chromatin-bound fraction after IR treatment (Fig. 6*F*). Consistent with a previous report (38), we observe that the chromatin-bound fraction of ATM is phosphorylated on Ser1981 after exposure to IR (Fig. 6*F*). Notably, the decrease in ATM levels at the chromatin fraction in KDM4D-depleted cells is not due to changes in the overall levels of ATM protein (Fig. 6*C*). Similar reduction in ATM levels at the chromatin-bound fraction was also observed in KDM4D-depleted cells treated with etoposide (Fig. 6*G*). Altogether, our data suggest that the defective association of ATM with chromatin in KDM4D-depleted cells could contribute to inefficient phosphorylation of a subset of ATM substrates.

KDM4D Affects the IR-Induced Foci Formation of Rad51 and 53BP1 Proteins. KDM4D depletion impairs the phosphorylation of KAP1-Ser824, which is known to facilitate DSB repair (6, 39, 40). On this basis, we decided to investigate foci formation of Rad51, a central protein involved in homology-directed repair

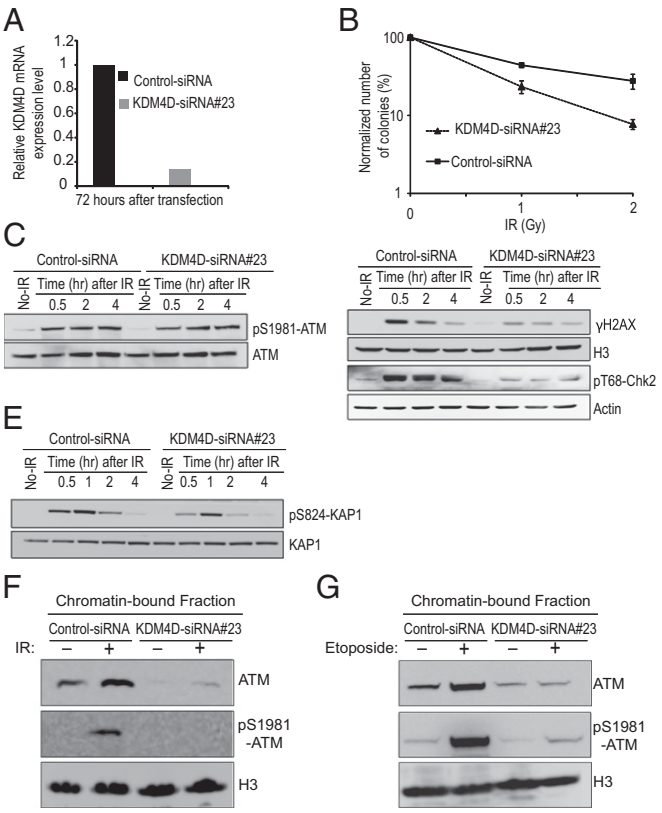

Fig. 6. KDM4D promotes cell survival and facilitates the DNA damage-induced phosphorylation of a subset of ATM substrates. (*A*) Nearly 85% KDM4D knockdown as confirmed using TaqMan real-time PCR. (*B*) Clonogenic assay shows that KDM4D depletion sensitizes cells to IR. Control and KDM4D-depleted cells were seeded at a density of 600 cells per 6-cm plate and exposed to increasing doses of IR. Plates were stained with crystal violet, and the numbers of surviving colonies were evaluated 12 d after irradiation. The averages of total colony numbers were done in triplicate and are representative of two independent experiments. The numbers of colonies were normalized to the percentage of undamaged cells and plotted as a function of IR dosage. Error bars represent the SEM in two independent experiments. (*C–E*) KDM4D knockdown impairs the phosphorylation of H2AX-S139, KAP1-S824, and Chk2-T68 but has no detectable effect on the phosphorylation of ATM-S1981 protein. Control and KDM4D-depleted U2OS cells were exposed to IR (5 Gy), and protein extracts were prepared at the indicated time points using a hot-lysis procedure and subjected to Western blotting using antibodies against the indicated proteins. Next, the membranes were stripped and reacted with anti-H3, ATM, KAP1, and actin for loading controls. These results are representative of two independent experiments. (*F*) KDM4D depletion impairs the association of ATM with chromatin. Control and KDM4D siRNA-transfected U2OS cells were exposed to IR (5 Gy) and subjected to cellular fractionation. Chromatin-bound fractions were immunoblotted using the indicated antibodies. (*G*) As in *F*, except that the cells were exposed to either DMSO or etoposide before cellular fractionation. Results shown in *F* and *G* are representative of at least two independent experiments.

(HDR) of DSBs, and 53BP1 foci formation that facilitates DSB repair by NHEJ. To do so, KDM4D was knocked down using two different siRNA sequences, sequences 23 and 24. Mock and KDM4D-depleted cells were seeded in 96-well plates and exposed to 3 Gys IR. Next, cells were fixed at the indicated time points after IR and stained for γH2AX, Rad51, and 53BP1. Automatic acquisition of 500 cells from each time point was carried out using a high-content screening microscope. Results show that KDM4D knockdown leads to a significant reduction in the intensity of γH2AX (Fig. 7*A*). These observations are consistent with the decrease in H2AX phosphorylation that was evident by Western blot analysis following KDM4D depletion (Fig. 6*D*). Interestingly, KDM4D depletion also leads to a dramatic decrease in the percentage of cells showing more than three Rad51 foci (Fig. 7*B*). Similarly, KDM4D depletion reduces the DNA damage-induced 53BP1 foci (Fig. 7*C*). Collectively, these observations indicate that KDM4D promotes Rad51 and 53BP1 foci formation and implicate KDM4D in DSB repair.

The Demethylase Activity and the Recruitment of KDM4D to Sites of DNA Damage Are both Required for Intact HDR of DSBs. The defective formation of Rad51 foci after damage prompted us to investigate the integrity of HDR of DSB in vivo. Toward this end, we used U2OS-HR-ind cells that form DSB at the I-Sce-I site within the GFP expression cassette following the addition of Dex. Repairing the DSBs by HDR restores the integrity of the GFP gene and leads to the appearance of GFP-positive cells (34). Control and KDM4D-siRNA–transfected HR-ind cells were treated with 0.1 μM Dex for 48 h, and the percentage of GFP-positive cells was determined by flow cytometry. Results show that depletion of KDM4D using two different siRNAs leads to a decrease of 29–34% in GFP-positive cells compared with control siRNA-treated cells. In addition, ATM kinase was used as a positive control for this assay, and its inhibition results in 61% decrease in the GFP-positive cells (Fig. 7*D*). Given that HDR functions only in the S and G2 phases of the cell cycle (2), we sought to test whether the decrease in the efficiency of HDR in KDM4D-depleted cells did not result from changes in cell-cycle distribution. Flow-cytometric analysis reveals that the depletion of KDM4D has no significant effect on cell-cycle distribution (Fig. 7*E*). We concluded therefore that the defective HDR of I-Sce-I–induced DSBs in KDM4D-depleted cells is not a consequence of cell accumulation at the G1 phase of the cell cycle.

To gain more insight into how KDM4D affects HDR of DSBs, we complemented KDM4D-depleted cells with constructs expressing DsRed-Monomere fused to siRNA-resistant forms of KDM4D-WT, KDM4D-S200M, or KDM4D-4M. Next, Dex was added to induce DSB, and the percentage of green cells out of red cells was determined using a flow cytometer. Strikingly, whereas the defect in DSB repair in KDM4D-deficient cells was mended by expressing wild-type KDM4D, both the KDM4D-S200M and KDM4D-4M mutants fail to restore the integrity of HDR (Fig. 7*F*). Altogether, these observations provide evidence that both the demethylase activity and the recruitment of KDM4D are required for intact HDR of DSBs.

The requirement of the demethylase activity of KDM4D for HDR was also established following the inhibition of KDM4 activity using the 8-hydroxyquinoline (8-HQ) molecule, which has been recently shown to inhibit the demethylase activity of the KDM4 family (41). We first validated that the 8-HQ compound can inhibit the demethylase activity of the KDM4D isoform. To do so, 8-HQ was added to doxycycline-treated U2OS-TetON-EGFP-KDM4D cells, and the levels of H3K9me3 were assessed by Western blotting. Results show that overexpression of EGFP-KDM4D leads to a decrease in the overall level of H3K9me3, which was inhibited in cells treated with 8-HQ molecules (Fig. 7*G*). We thus concluded that 8-HQ can effectively inhibit the demethylase activity of KDM4D. Next, U2OS-HR-ind cells were treated with increasing concentrations (50–100 μM) of 8-HQ, and the percentage of GFP-positive cells was determined by flow cytometery at 48 h following the addition of 0.1 μM Dex. Interestingly, we found that the percentage of GFP-positive cells decreases in a dose-dependent manner of 8-HQ inhibitor (between 31% and 73%) (Fig. 7*H*). This result suggests that the demethylase activity of KDM4 facilitates HDR of DSBs. Altogether; these data imply that normal HDR of DSBs requires intact demethylase activity of KDM4D protein.

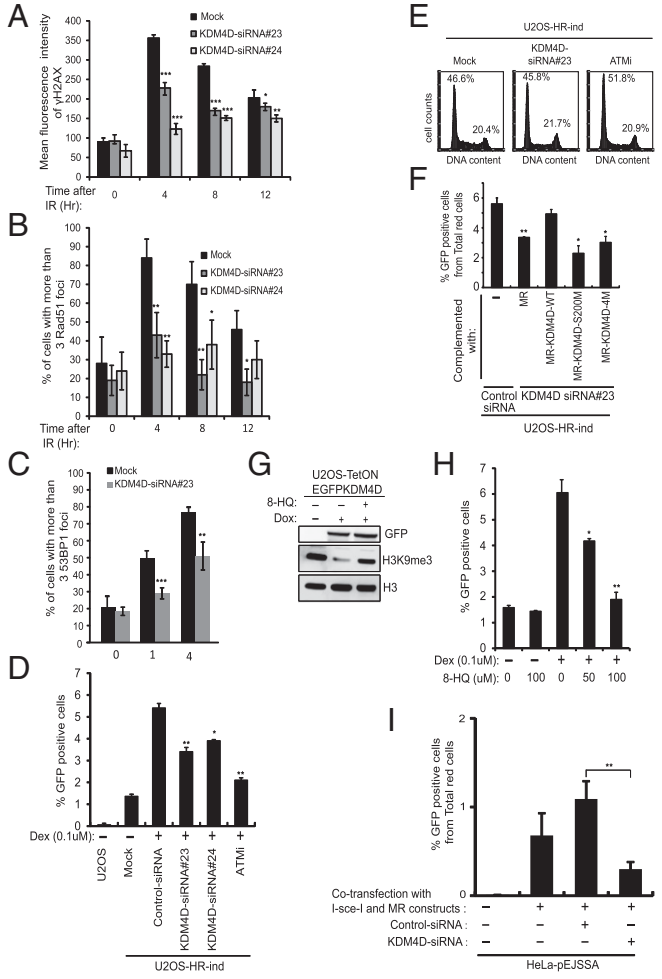

Fig. 7. KDM4D depletion affects double-strand break repair. (*A–C*) KDM4D was depleted from U2OS cells using two different siRNA sequences. Control siRNA was used as a negative control. Cells were seeded in 96-well plates and treated with 40 μM etoposide for 20 min. The drug was then removed, and cells were fixed at the indicated time points after DNA damage and immunostained with γH2AX, Rad51, and 53BP1. A high-content screening microscope (In Cell Analyzer 2000; GE Healthcare) was used for automatic acquisition of at least 500 cells at each time point. (*A*) The nuclear intensity of γH2AX was calculated using the IN Cell Analyzer Workstation 3.7. (*B*) The percentage of cells with more than three Rad51 foci. Results are typical of two independent experiments. Error bars show SDs from the mean. (*C*) The percentage of cells with more than three 53BP1 foci. (*D*) KDM4D depletion impairs HDR of DSBs induced by I-Sce-I endonuclease. A decrease of 29–34% in the GFP-positive cells was observed following the depletion of KDM4D in HR-ind cells. Results shown are typical of three independent experiments. For positive control, ATM was inhibited using 20 μM KU-55933. Two independent experiments show that ATM inhibition leads to 61% reduction in the GFP-positive cells. Error bars represent the SD. (*E*) Flow-cytometric analysis shows that KDM4D depletion or ATM inhibition has no significant effect on cell-cycle distribution. (*F*) The defects in HDR in KDM4D-deficient cells were mended by expressing wild-type KDM4D, but not KDM4D-S200M or KDM4D-4M mutants. Control and KDM4D-siRNA transfected HR-ind cells were transfected with constructs expressing the indicated forms of KDM4D and treated with 0.1 μM Dex for 48 h, and the percentage of GFP-positive cells from the total number of red cells was determined by flow cytometry. Results shown are typical of two independent experiments. Error bars represent SD. (*G*) The 8-hydroxyquinoline (8-HQ) molecule inhibits the demethylase activity of KDM4D. U2OS-TetON cells expressing EGFP-KDM4D cells were treated with 50 μM 8-HQ inhibitor for 12 h, and protein extracts were prepared using a hot-lysis procedure and subjected for Western blotting using GFP, H3K9me3, and H3 antibodies. (*H*) Chemical inhibition of KDM4 proteins impairs HDR of DSBs in a dose-dependent manner of 8-HQ. U2OS-HR-ind cells were incubated with increasing concentrations of 8-HQ for 2 h and then treated with 0.1 μM Dex for 48 h to induce the formation of I-Sce1 DSBs. To evaluate the integrity of HDR, cells were harvested, and the percentages of GFP-positive cells were determined using flow-cytometric analysis. Results shown are typical of two independent experiments. Error bars represent SD. (*I*) KDM4D depletion disrupts the integrity of NHEJ in vivo. A decrease of 65% in the GFP-positive cells was observed following the depletion of KDM4D in HeLa cells containing the NHEJ reporter, pEJSSA. Control and KDM4D siRNA-treated cells were cotransfected with constructs expressing I-Sce-I endonuclease and Red-Monomer (MR) tag. To evaluate the integrity of NHEJ, cells were harvested, and the percentage of GFP-positive cells from the total number of red cells was determined by flow cytometry. Results shown are typical of two independent experiments. Error bars represent the SD. The *P* values were calculated using two-tailed paired tests, compared with control of each time point. *, **, and *** indicate significance at $P < 0.05$, 0.01, and 0.001, respectively.

KDM4D Promotes NHEJ of DSB. We have shown that KDM4D enhances the timely formation of 53BP1 foci upon DNA damage (Fig. 7*C*). Knowing that 53BP1 facilitates DSB repair by the NHEJ pathway (42, 43), we reasoned that KDM4D might also affect NHEJ of DSBs. To assess this possibility, HeLa cells containing the plasmid pEJSSA stably integrated into their genome were used to monitor the efficiency of NHEJ in vivo. This plasmid contains a recognition site for I-Sce-I endonucleases, and the repair of the DSB by NHEJ leads to the appearance of green fluorescent cells (44). Control and KDM4D siRNA-treated cells were cotransfected with vectors expressing I-SceI endonuclease and RedMonomer tag as a control for transfection efficiency. Cells were left for 48 h, and then the ratio of GFP-positive cells out of the RedMonomer-positive cells was determined using a BD LSRII flow cytometer. Results show that KDM4D depletion leads to an ∼65% decrease in the efficiency of NHEJ of DSBs (Fig. 7*I*). Collectively, our results suggest that KDM4D regulates the integrity of HDR and NHEJ of DSBs.

In summary, this study shows that the PARP1-dependent recruitment of KDM4D to sites of DNA damage promotes the phosphorylation of particular ATM substrates and facilitates the formation of Rad51 and 53BP1 foci. Moreover, we have shown that KDM4D promotes the association of ATM with chromatin, thus providing mechanistic insight into the mechanism by which KDM4D ablation impairs the repair of DSBs.

Discussion

KDM4D belongs to the KDM4 family that demethylates H3K9me2/me3 marks and consists of evolutionarily conserved JmjN and JmjC domains at its N terminus whereas the overall sequence of C-terminal region contains no obvious characterized domains (16). This study revealed that KDM4D is swiftly recruited to sites of damage in a PARP1-dependent manner. Moreover, we show that KDM4D promotes the phosphorylation of early DNA damage markers and also facilitates the formation of Rad51 and 53BP1 foci. Consequently, KDM4D depletion affects the integrity of HDR and NHEJ of DSBs. These results uncover an unprecedented role of KDM4D lysine demethylase in DNA damage repair of DSBs.

Our data implicate KDM4D in the early events of DDR, as it promotes the phosphorylation H2AX, the earliest known marker of DNA damage (Figs. 6*D* and 7*A*). How does KDM4D influence H2AX phosphorylation? ATM levels at chromatin are known to increase in response to DNA damage (38). Here, we show that KDM4D inhibits the DNA damage-dependent increase in ATM at chromatin (Fig. 6*F*), thereby impeding the accessibility of ATM kinase to its chromatin substrates, providing a possible explanation for the impairment of H2AX phosphorylation. Subsequently, the reduction in KAP1 and Chk2 phosphorylation and the impairment of Rad51 and 53BP1 foci formation in KDM4D-depleted cells can be a consequence of the inefficient phosphorylation of H2AX. Alternatively, KDM4D

activity can directly promote the phosphorylation and the foci formation of these downstream targets of DNA damage.

A key question is how KDM4D facilitates the localization of ATM at chromatin. One possibility is that KDM4D-dependent demethylation of ATM is involved in its retention at chromatin. Second is that KDM4D might serve as a scaffold protein for recruiting ATM to chromatin. However, immunoprecipitation experiments show that KDM4D does not interact with ATM kinase, indicating that the alleged ATM–KDM4D interaction is either weak or transient and is likely lost during pull-down assays. Third is that the demethylase activity of KDM4D facilitates the accessibility of ATM kinase to its substrates, which can be achieved by relaxing the chromatin structure through local demethylation of H3K9me2/me3 surrounding the DNA damage sites. Indeed, it was shown that the levels of H3K9me2/3 in γH2AX-positive regions decrease after damage (29, 45).

Our results show that PARP1 regulates KDM4D recruitment to sites of DNA damage (Figs. 3–5), suggesting that both proteins might act in the same pathway of DDR. However, whereas KDM4D depletion reduces HDR of DSB, PARP1 inhibition results in hyper recombination (46). These apparently controversial observations can be due to the fact that KDM4D and PARP1 have distinct functions that are independent of each other. Therefore, we do not necessarily anticipate that PARP1 depletion phenotype phenocopies the phenotype of KDM4D depletion. Indeed, PARP1 depletion does not phenocopy depletion of meiotic recombination 11 homolog (MRE11), another protein in the DNA damage response that depends on PARylation for recruitment (47). Interestingly, our results are consistent with recent evidence showing that the depletion of MRE11, Nijmegen breakage syndrome 1, and chromodomain helicase DNA binding protein 4 (CHD4) proteins, whose recruitment to sites of DNA damage is regulated by PARP1, disrupts the HDR of DSB (47–49). Moreover, the rapid and transient recruitment of KDM4D to sites of DNA damage is in line with the increasing numbers of DDR proteins that show transient recruitment, but long lasting effect on repair and/or DNA damage-induced foci formation (49–55).

PARP1 is known to modulate chromatin structure at DNA damage sites by PARylating histones (56) and nonhistone proteins (57–60). Here, we suggest that PARP1 modifies chromatin structure also through recruiting KDM4D histone demethylase to sites of DNA damage. Similarly, it was recently shown that PARP1 and Really Interesting New Gene finger protein (RNF)8 ubiquitin ligase regulate the recruitment of the catalytic subunit of the NuRD repressor complex, CHD4, to DNA-breakage sites (49, 61). CHD4 recruitment to sites of DNA damage is much slower (5 min) compared with KDM4D recruitment (15 s), suggesting that KDM4D may function upstream of CHD4.

Many of the DNA damage repair proteins form immunofluorescence-detectable foci in response to DNA damage. Interestingly, no such foci of KDM4D were formed in response to IR or after exposing cells to genotoxic agents. This observation is similar to the behavior of other known DDR proteins, such as CHD4 (49), Lupus Ku autoantigen protein P70 (Ku70), Lupus Ku autoantigen protein P86 (Ku86) (62), RNF4 (63), and heterochromatin protein 1 (HP1) (5, 64), that remain diffuse throughout the nucleus in response to IR. Nevertheless, we were able to convincingly show KDM4D recruitment to a single double strand break generated by I-Sce-I endonuclease.

Many of the DNA damage repair proteins form immunofluorescence-detectable foci in response to DNA damage. Interestingly, no such foci of KDM4D were formed in response to IR or after exposing cells to genotoxic agents, such as etoposide. Nevertheless, we were able to convincingly show that KDM4D accumulates at etoposide-damaged chromatin (Fig. 1*F*) and is recruited to DSBs generated by I-Sce-I endonuclease (Fig. 1*G*). This behavior is similar to other known DDR proteins, such as CHD4 (49), Ku70, Ku86 (62), RNF4 (63), and HP1 (5, 64), that remain diffuse throughout the nucleus in response to IR or genotoxic treatments but show accumulation at damaged chromatin (49, 65, 66) and are recruited to I-Sce-I–induced DSBs (67). The inability to visualize DNA damage-induced foci by conventional immunofluorescence could be therefore due to technical obstacles rather than lack of recruitment to damaged chromatin.

How does KDM4D facilitate DSBs repair? Our data suggest that the defective HDR and NHEJ in KDM4D-depleted cells is likely to be caused by the inefficient formation of Rad51 and 53BP1 foci. In support of this suggestion, several published reports show that inhibition of Rad51 foci formation disrupts the HDR integrity of DSB (68–70) and that knockdown of 53BP1 impairs NHEJ (42, 43).

In summary, here, we present previously unidentified evidence linking KDM4D histone demethylase to the initiation of the DNA damage-signaling cascade and to the repair of DSBs. Importantly, we demonstrate that KDM4D is critical for the association of ATM with chromatin, thus providing a possible explanation for the impaired phosphorylation of ATM substrates. Identifying KDM4D histone demethylase as an additional player in DSB repair will help us to better understand the molecular mechanisms that ensure efficient repair of DNA lesions to maintain genomic stability.

Materials and Methods

In Vitro PARylation Assay. His-tagged wild-type, N-terminal, C-terminal, and different mutants of KDM4D (0.125 mg) were subjected to in vitro PARylation at room temperature for 20 min in a reaction buffer (50 mM Tris·HCl, pH 8, 25 mM $MgCl_2$, 50 mM NaCl) supplemented with 200 μM NAD^+, activated DNA, and PARP1 enzyme (Trevigen). The reaction was stopped by adding 5× SDS/PAGE sample buffer and subjected to Western blot analysis.

In Vitro Histone Demethylation Assay. The histone demethylation assay was performed as previously described (19). Briefly, 5 μg of bulk histones (Sigma) were incubated with 5 μg of purified His-tagged KDM4D proteins in a demethylation buffer (20 mM Tris, pH 7.3, 150 mM NaCl, 1 mM α-ketoglutarate, 50 μM $FeSO_4$, 2 mM ascorbic acid) at 37 °C overnight. Reaction mixtures were resolved in gel and analyzed by Western blotting using H3K9me3 and H3 specific antibodies.

Homology-Directed Repair Assay. The efficiency of homology-directed repair of DSBs was performed as previously described (34). In brief, U2OS-HR-ind cells, which stably express cytoplasmic mCherry-I-Sce-I enzyme fused to glucocorticoid receptor (I-Sce-I-GR), were treated with 0.1 μM dexamethasone (Dex) for 48 h. This treatment induced rapid entry of I-Sce-I-GR into the nucleus and generation of DSB at its recognition sequence within the reporter construct expressing GFP. Repairing the DSB by HDR restored the integrity of the GFP gene. To measure the GFP-positive cells, U2OS-HR-ind cells were trypsinized and washed once with PBS×1 and then resuspended in PBS×1 containing 7% FBS. The number of GFP-positive cells was determined using a BD LSRII. Data analysis was performed using FCS-Express software and was based on at least 50,000 events. Because the I-Sce-I-GR is stably expressed, no normalization was required.

Laser Microirradiation. Cells were presensitized with 10 μM Hoechst 3334 dye for 15 min at 37 °C. Then, laser microirradiation was performed using an inverted confocal microscope (LSM-700; Zeiss) equipped with a CO_2 module and a 37 °C heating chamber. A preselected spot within the nucleus was microirradiated with 10 iterations of a 405-nm laser with 100% power to generate localized DNA damage. Then, either cells were fixed for immunofluorescence, or time-lapse images were acquired using a 488-nm laser at 15-s time intervals. The fluorescence intensity of EGFP signals at laser-microirradiated sites was measured using Zen 2009 software (Carl Zeiss). Data obtained were corrected for the loss of total fluorescence and normalized to the initial intensity.

ACKNOWLEDGMENTS. We thank Yosef Shiloh (Tel Aviv University) for the generous gifts of the HeLa-pEJSSA cell line, KAP1, and ATM antibodies and for helpful suggestions and comments. We thank Karnit Barat and Ilana Kupershmit for help in constructing plasmids used in this study. We thank Michal Goldberg (Hebrew University, Jerusalem, Israel) for the U2OS-HR-ind cell line and Vera Gorbunova (University of Rochester) for the HCA-2 cell line. We thank Michele Rouleau (Laval University) for the plasmids encoding EGFP-

PARP1. We thank Fabian Glaser for his help in preparing Fig. 4*A* and Sara Selig and Shira Urim for critical reading of the manuscript. We thank Maayan Duvshani-Eshet, Nitzan Dahan, and Efrat Barak (Life Sciences and Engineering Infrastructure Unit, Technion) for help in the microscopy and flow cytometry-related work. Research in the N.A. laboratory is supported by grants from the Israel Cancer Research Fund, the Israel Science Foundation, the Israel Cancer Association, the H. Blechman Memorial Cancer Research Fund, and the Eliayahu Pen Research Fund.

1. Jackson SP, Bartek J (2009) The DNA-damage response in human biology and disease. *Nature* 461(7267):1071–1078.
2. Hartlerode AJ, Scully R (2009) Mechanisms of double-strand break repair in somatic mammalian cells. *Biochem J* 423(2):157–168.
3. Venkitaraman AR (2010) Modifying chromatin architecture during the response to DNA breakage. *Crit Rev Biochem Mol Biol* 45(1):2–13.
4. Polo SE, Jackson SP (2011) Dynamics of DNA damage response proteins at DNA breaks: A focus on protein modifications. *Genes Dev* 25(5):409–433.
5. Ayoub N, Jeyasekharan AD, Bernal JA, Venkitaraman AR (2008) HP1-beta mobilization promotes chromatin changes that initiate the DNA damage response. *Nature* 453(7195):682–686.
6. Ziv Y, et al. (2006) Chromatin relaxation in response to DNA double-strand breaks is modulated by a novel ATM- and KAP-1 dependent pathway. *Nat Cell Biol* 8(8):870–876.
7. Pei H, et al. (2011) MMSET regulates histone H4K20 methylation and 53BP1 accumulation at DNA damage sites. *Nature* 470(7332):124–128.
8. Shi X, et al. (2007) Modulation of p53 function by SET8-mediated methylation at lysine 382. *Mol Cell* 27(4):636–646.
9. Huang J, et al. (2007) p53 is regulated by the lysine demethylase LSD1. *Nature* 449(7158):105–108.
10. Sun Y, et al. (2009) Histone H3 methylation links DNA damage detection to activation of the tumour suppressor Tip60. *Nat Cell Biol* 11(11):1376–1382.
11. Chuikov S, et al. (2004) Regulation of p53 activity through lysine methylation. *Nature* 432(7015):353–360.
12. Kouzarides T (2007) Chromatin modifications and their function. *Cell* 128(4):693–705.
13. Peters AH, et al. (2001) Loss of the Suv39h histone methyltransferases impairs mammalian heterochromatin and genome stability. *Cell* 107(3):323–337.
14. Kamakaka RT, Biggins S (2005) Histone variants: Deviants? *Genes Dev* 19(3):295–310.
15. Schotta G, et al. (2004) A silencing pathway to induce H3-K9 and H4-K20 trimethylation at constitutive heterochromatin. *Genes Dev* 18(11):1251–1262.
16. Klose RJ, Kallin EM, Zhang Y (2006) JmjC-domain-containing proteins and histone demethylation. *Nat Rev Genet* 7(9):715–727.
17. Shi Y, Whetstine JR (2007) Dynamic regulation of histone lysine methylation by demethylases. *Mol Cell* 25(1):1–14.
18. Cloos PA, et al. (2006) The putative oncogene GASC1 demethylates tri- and dimethylated lysine 9 on histone H3. *Nature* 442(7100):307–311.
19. Whetstine JR, et al. (2006) Reversal of histone lysine trimethylation by the JMJD2 family of histone demethylases. *Cell* 125(3):467–481.
20. Chen Z, et al. (2006) Structural insights into histone demethylation by JMJD2 family members. *Cell* 125(4):691–702.
21. Black JC, Van Rechem C, Whetstine JR (2012) Histone lysine methylation dynamics: Establishment, regulation, and biological impact. *Mol Cell* 48(4):491–507.
22. Kooistra SM, Helin K (2012) Molecular mechanisms and potential functions of histone demethylases. *Nat Rev Mol Cell Biol* 13(5):297–311.
23. Shi L, et al. (2011) Histone demethylase JMJD2B coordinates H3K4/H3K9 methylation and promotes hormonally responsive breast carcinogenesis. *Proc Natl Acad Sci USA* 108(18):7541–7546.
24. Yang J, et al. (2010) The histone demethylase JMJD2B is regulated by estrogen receptor alpha and hypoxia, and is a key mediator of estrogen induced growth. *Cancer Res* 70(16):6456–6466.
25. Gray SG, et al. (2005) Functional characterization of JMJD2A, a histone deacetylase- and retinoblastoma-binding protein. *J Biol Chem* 280(31):28507–28518.
26. Fodor BD, et al. (2006) Jmjd2b antagonizes H3K9 trimethylation at pericentric heterochromatin in mammalian cells. *Genes Dev* 20(12):1557–1562.
27. Black JC, et al. (2013) KDM4A lysine demethylase induces site-specific copy gain and rereplication of regions amplified in tumors. *Cell* 154(3):541–555.
28. Palomera-Sanchez Z, Bucio-Mendez A, Valadez-Graham V, Reynaud E, Zurita M (2010) Drosophila p53 is required to increase the levels of the dKDM4B demethylase after UV-induced DNA damage to demethylate histone H3 lysine 9. *J Biol Chem* 285(41): 31370–31379.
29. Young LC, McDonald DW, Hendzel MJ (2013) Kdm4b histone demethylase is a DNA damage response protein and confers a survival advantage following γ-irradiation. *J Biol Chem* 288(29):21376–21388.
30. Mallette FA, et al. (2012) RNF8- and RNF168-dependent degradation of KDM4A/JMJD2A triggers 53BP1 recruitment to DNA damage sites. *EMBO J* 31(8):1865–1878.
31. Smeenk G, et al. (2010) The NuRD chromatin-remodeling complex regulates signaling and repair of DNA damage. *J Cell Biol* 190(5):741–749.
32. Huda N, et al. (2012) Recruitment of TRF2 to laser-induced DNA damage sites. *Free Radic Biol Med* 53(5):1192–1197.
33. Mao Z, et al. (2011) SIRT6 promotes DNA repair under stress by activating PARP1. *Science* 332(6036):1443–1446.
34. Shahar OD, et al. (2012) Live imaging of induced and controlled DNA double-strand break formation reveals extremely low repair by homologous recombination in human cells. *Oncogene* 31(30):3495–3504.
35. Krishnakumar R, Kraus WL (2010) The PARP side of the nucleus: Molecular actions, physiological outcomes, and clinical targets. *Mol Cell* 39(1):8–24.
36. Le May N, et al. (2012) Poly (ADP-ribose) glycohydrolase regulates retinoic acid receptor-mediated gene expression. *Mol Cell* 48(5):785–798.
37. So S, Davis AJ, Chen DJ (2009) Autophosphorylation at serine 1981 stabilizes ATM at DNA damage sites. *J Cell Biol* 187(7):977–990.
38. Kim YC, et al. (2009) Activation of ATM depends on chromatin interactions occurring before induction of DNA damage. *Nat Cell Biol* 11(1):92–96.
39. Goodarzi AA, et al. (2008) ATM signaling facilitates repair of DNA double-strand breaks associated with heterochromatin. *Mol Cell* 31(2):167–177.
40. Noon AT, et al. (2010) 53BP1-dependent robust localized KAP-1 phosphorylation is essential for heterochromatic DNA double-strand break repair. *Nat Cell Biol* 12(2):177–184.
41. King ON, et al. (2010) Quantitative high-throughput screening identifies 8-hydroxyquinolines as cell-active histone demethylase inhibitors. *PLoS ONE* 5(11):e15535.
42. Difilippantonio S, et al. (2008) 53BP1 facilitates long-range DNA end-joining during V(D)J recombination. *Nature* 456(7221):529–533.
43. Dimitrova N, Chen YC, Spector DL, de Lange T (2008) 53BP1 promotes non-homologous end joining of telomeres by increasing chromatin mobility. *Nature* 456(7221):524–528.
44. Mansour WY, et al. (2008) Hierarchy of nonhomologous end-joining, single-strand annealing and gene conversion at site-directed DNA double-strand breaks. *Nucleic Acids Res* 36(12):4088–4098.
45. Falk M, Lukasova E, Gabrielova B, Ondrej V, Kozubek S (2007) Chromatin dynamics during DSB repair. *Biochim Biophys Acta* 1773(10):1534–1545.
46. Schultz N, Lopez E, Saleh-Gohari N, Helleday T (2003) Poly(ADP-ribose) polymerase (PARP-1) has a controlling role in homologous recombination. *Nucleic Acids Res* 31(17):4959–4964.
47. Haince JF, et al. (2008) PARP1-dependent kinetics of recruitment of MRE11 and NBS1 proteins to multiple DNA damage sites. *J Biol Chem* 283(2):1197–1208.
48. Pan MR, et al. (2012) Chromodomain helicase DNA-binding protein 4 (CHD4) regulates homologous recombination DNA repair, and its deficiency sensitizes cells to poly (ADP-ribose) polymerase (PARP) inhibitor treatment. *J Biol Chem* 287(9):6764–6772.
49. Polo SE, Kaidi A, Baskcomb L, Galanty Y, Jackson SP (2010) Regulation of DNA-damage responses and cell-cycle progression by the chromatin remodelling factor CHD4. *EMBO J* 29(18):3130–3139.
50. Adamson B, Smogorzewska A, Sigoillot FD, King RW, Elledge SJ (2012) A genome-wide homologous recombination screen identifies the RNA-binding protein RBMX as a component of the DNA-damage response. *Nat Cell Biol* 14(3):318–328.
51. Yan Q, et al. (2013) BAL1 and its partner E3 ligase, BBAP, link Poly(ADP-ribose) activation, ubiquitylation, and double-strand DNA repair independent of ATM, MDC1, and RNF8. *Mol Cell Biol* 33(4):845–857.
52. Altmeyer M, et al. (2013) The chromatin scaffold protein SAFB1 renders chromatin permissive for DNA damage signaling. *Mol Cell* 52(2):206–220.
53. Mastrocola AS, Kim SH, Trinh AT, Rodenkirch LA, Tibbetts RS (2013) The RNA-binding protein fused in sarcoma (FUS) functions downstream of poly(ADP-ribose) polymerase (PARP) in response to DNA damage. *J Biol Chem* 288(34):24731–24741.
54. Mosammaparast N, et al. (2013) The histone demethylase LSD1/KDM1A promotes the DNA damage response. *J Cell Biol* 203(3):457–470.
55. Krietsch J, et al. (2012) PARP activation regulates the RNA-binding protein NONO in the DNA damage response to DNA double-strand breaks. *Nucleic Acids Res* 40(20): 10287–10301.
56. Boulikas T (1988) At least 60 ADP-ribosylated variant histones are present in nuclei from dimethylsulfate-treated and untreated cells. *EMBO J* 7(1):57–67.
57. Pines A, et al. (2012) PARP1 promotes nucleotide excision repair through DDB2 stabilization and recruitment of ALC1. *J Cell Biol* 199(2):235–249.
58. Luijsterburg MS, et al. (2012) DDB2 promotes chromatin decondensation at UV-induced DNA damage. *J Cell Biol* 197(2):267–281.
59. Chou DM, et al. (2010) A chromatin localization screen reveals poly (ADP ribose)-regulated recruitment of the repressive polycomb and NuRD complexes to sites of DNA damage. *Proc Natl Acad Sci USA* 107(43):18475–18480.
60. Ahel D, et al. (2009) Poly(ADP-ribose)-dependent regulation of DNA repair by the chromatin remodeling enzyme ALC1. *Science* 325(5945):1240–1243.
61. Luijsterburg MS, et al. (2012) A new non-catalytic role for ubiquitin ligase RNF8 in unfolding higher-order chromatin structure. *EMBO J* 31(11):2511–2527.
62. Mirzoeva OK, Petrini JH (2001) DNA damage-dependent nuclear dynamics of the Mre11 complex. *Mol Cell Biol* 21(1):281–288.
63. Galanty Y, Belotserkovskaya R, Coates J, Jackson SP (2012) RNF4, a SUMO-targeted ubiquitin E3 ligase, promotes DNA double-strand break repair. *Genes Dev* 26(11):1179–1195.
64. Ayoub N, Jeyasekharan AD, Venkitaraman AR (2009) Mobilization and recruitment of HP1: A bimodal response to DNA breakage. *Cell Cycle* 8(18):2945–2950.
65. Luo K, Zhang H, Wang L, Yuan J, Lou Z (2012) Sumoylation of MDC1 is important for proper DNA damage response. *EMBO J* 31(13):3008–3019.
66. Calkins AS, Iglehart JD, Lazaro JB (2013) DNA damage-induced inhibition of rRNA synthesis by DNA-PK and PARP-1. *Nucleic Acids Res* 41(15):7378–7386.
67. Ogiwara H, et al. (2011) Histone acetylation by CBP and p300 at double-strand break sites facilitates SWI/SNF chromatin remodeling and the recruitment of non-homologous end joining factors. *Oncogene* 30(18):2135–2146.
68. Pierce AJ, Johnson RD, Thompson LH, Jasin M (1999) XRCC3 promotes homology-directed repair of DNA damage in mammalian cells. *Genes Dev* 13(20):2633–2638.
69. Bishop DK, et al. (1998) Xrcc3 is required for assembly of Rad51 complexes in vivo. *J Biol Chem* 273(34):21482–21488.
70. Budke B, et al. (2012) RI-1: A chemical inhibitor of RAD51 that disrupts homologous recombination in human cells. *Nucleic Acids Res* 40(15):7347–7357.